Geomechanics and Engineering, *Vol. 10, No. 2 (2016) 225-245*
DOI: http://dx.doi.org/10.12989/gae.2016.10.2.225

A novel modeling of settlement of foundations in permafrost regions

Songhe Wang [*1], Jilin Qi [2], Fan Yu [3] and Fengyin Liu [1]

[1] *Institute of Geotechnical Engineering, Xi'an University of Technology, Xi'an Shaanxi, 710048, China*
[2] *College of Civil and Transportation Engineering, Beijing University of Civil Engineering and Architecture, Beijing 100044, China*
[3] *State Key Laboratory of Frozen Soil Engineering, Cold and Arid Regions Environmental and Engineering Research Institute, Chinese Academy of Sciences, Lanzhou Gansu 730000, China*

(*Received April 29, 2015, Revised December 07, 2015, Accepted December 10, 2015*)

Abstract. Settlement of foundations in permafrost regions primarily results from three physical and mechanical processes such as thaw consolidation of permafrost layer, creep of warm frozen soils and the additional deformation of seasonal active layer induced by freeze-thaw cycling. This paper firstly establishes theoretical models for the three sources of settlement including a statistical damage model for soils which experience cyclic freeze-thaw, a large strain thaw consolidation theory incorporating a modified Richards' equation and a Drucker-Prager yield criterion, as well as a simple rheological element based creep model for frozen soils. A novel numerical method was proposed for live computation of thaw consolidation, creep and freeze-thaw cycling in corresponding domains which vary with heat budget in frozen ground. It was then numerically implemented in the FISH language on the FLAC platform and verified by freeze-thaw tests on sandy clay. Results indicate that the calculated results agree well with the measured data. Finally a model test carried out on a half embankment in laboratory was modeled.

Keywords: settlement; frozen ground; freeze-thaw; thaw consolidation; creep

1. Introduction

Since the past century, lifeline projects such as highways, railways, and oil and gas pipelines have been increasingly constructed in Northern China. Under dual effects of global climate change and increasing engineering activities, the engineering properties of frozen ground varied with heat budget (Lai *et al*. 2010a, b, Yu *et al*. 2013, Kanevskiy *et al*. 2013, Che *et al*. 2014), leading to a series of engineering problems in permafrost regions, e.g., settlement of foundations, frost boiling, cracks of pavement and thaw slumping of slopes (Wu *et al*. 2007, Wu and Zhang 2008, Yang *et al*. 2010); of which, the continuing settlement of foundations is a great challenge in geocryology and also poses potential threats to social and economic developments in permafrost regions (Qi *et al*. 2007, Ma *et al*. 2008a, 2009).

Settlement of foundations in permafrost regions is closely related to the engineering geological and atmospheric conditions (Qi *et al*. 2007). Firstly, frozen soil is sensitive to the heat budget due to ice inclusion. Tsytovich (1975) recommended the principles for frozen soil engineering design,

*Corresponding author, Ph.D., E-mail: wangsonghe@126.com

http://www.techno-press.org/?journal=gae&subpage=7 ISSN: 2005-307X (Print), 2092-6219 (Online)

i.e., keeping frozen, gradually thawing and pre-thawing. Some engineering techniques for permafrost protection have played a positive role in building the Qinghai-Tibet railway, e.g., riprap slope protection, ventilated embankment and thermosyphon (Cheng *et al*. 2008, Ma *et al*. 2008b, c). Secondly, settlement mechanism in permafrost foundations has been studied by many scholars. Qi *et al*. (2007) summarized from the monitored data in the Qinghai-Tibet plateau that three physical and mechanical processes were primarily involved in the settlement of permafrost foundations such as thaw consolidation of permafrost layer, creep of warm frozen soils and the additional deformation due to freeze-thaw cycling. Of which, thaw consolidation caused by continuing thawing of permafrost has always been considered as the primary source of settlement. As permafrost rises in temperature, creep of the newly formed warm permafrost beneath the permafrost table should also be considered (Qi *et al*. 2007). Moreover, the freeze-thaw can induce additional deformation in foundations by changing the engineering properties of soils (Qi *et al*. 2007, Kamei *et al*. 2012, Wang *et al*. 2015, Matsumura *et al*. 2015). Further field experimental studies indicate that the proportion of each source of settlement accounts for varies with the geological and geomorphological conditions (Yu *et al*. 2012).

When estimating settlement of foundations in permafrost regions, empirical methods such as the improved gray prediction model (Zhou and Tang 2015) and the elastoplastic model at high confining pressures (Yang *et al*. 2010) were primarily used. However, we can hardly obtain an accurate result by empirical methods due to the coupled effects of heat transfer, migration of water as well as the stress-strain responses. In most cases, we seek for approximate solutions by utilizing numerical methods such as the finite difference method (FDM) or the finite element method (FEM). As far as the heat transfer is concerned, two key problems should be solved, i.e., thermal boundary, and absorption and release of latent heat during phase change. For the former the effect of atmospheric circulation on ground surface can be simplified as a sinusoidal equation if meteorological data is sufficient while the latent heat released or absorbed during ice-water phase change can be simulated by introducing an alternative thermal index, e.g., enthalpy and equivalent specific heat (Ma *et al*. 2008c). Based on heat transfer results, the coupled processes of water migration and stress-strain responses, e.g., thaw consolidation of frozen ground, have been numerically investigated. Qi *et al*. (2012) put forward the concept of the effective consolidation time and established a 3-D large strain thaw consolidation model for thawing permafrost. Yao (Yao *et al*. 2012) proposed a large strain theory for the consolidation of thawing permafrost based on an Eulerian description-based strain rate and rotation rate. Qi *et al*. (2013) derived a three dimensional thaw consolidation theory combining the Biot's theory with heat conductive equations considering the ice-water phase change effects. For warm and ice-rich permafrost, creep should also be taken into account (Qi *et al*. 2007) and the built-in creep criterion is mostly used in computation, e.g., time-hardening law in ANSYS. Li *et al*. (2009a) deduced a moisture, heat and creep couple model to evaluate the long-term stability of Qinghai-Tibet Railway embankments. Moreover, some user-defined models can also be compiled by programming languages and called by the main program. Coupled with modules for thermal and dynamic computations, creep of frozen soils under complex boundaries can also be simulated (Li *et al*. 2009b, Wang *et al*. 2013). However, attention of previous work was mainly paid to a single source of settlement, which is far from enough for estimating settlement of foundations in permafrost regions.

This paper aims to propose a novel method for estimating settlement of foundations in permafrost regions by taking into account the three main sources of settlement such as thaw consolidation, creep, and freeze-thaw cycling. Firstly, the theoretical models for three sources of settlement will be established. After solving the primary technical problems, a novel method will

be numerically implemented in the FISH language on the FLAC platform. The method will then be verified by freeze-thaw tests on sandy clay taken from the Qinghai-Tibet plateau. Finally, an embankment model test will be modelled.

2. Governing equations

2.1 Freeze-thaw

The structural damage of geo-materials under load can be described by a statistical distribution function by incorporating the strength criterion for micro elements in materials, e.g., the normal distribution, the lognormal distribution and the Weibull distribution (Lai *et al*. 2008, Li *et al*. 2009c). Here, the damage variable D for the loading effect can be expressed as

$$D = \frac{N_t}{N} \tag{1}$$

where N_t and N are the numbers for the damaged and the total elements, respectively. It varies from 0 to 1 corresponding to the intact and completely damaged states, respectively.

We assumed a Weibull probability density function for the strength of micro-elements (Li *et al*. 2012) and when a certain magnitude of stress is applied, we can obtain a specific form of D

$$D = \frac{N_t}{N} = 1 - e^{-\left(\frac{F}{F_0}\right)^{\beta}} \tag{2}$$

where β is the shape parameter for the Weibull distribution denoting the degree of material homogeneity; and F_0 is the scale parameter associated with the strength of soil elements; F is the strength criterion for soil elements.

For most fine-grained soils the elastic modulus after freeze-thaw decreases, which is closely related to the micro-structural changes of soils after freeze-thaw, e.g., growth of micro-fracture and development of macro-pores (Qi *et al*. 2006). Moreover, the elastic modulus can be conveniently determined by test. Thus, we used the following damage variable D_n

$$D_n = 1 - \frac{E_n}{E_0} \tag{3}$$

where E_0 and E_n are the elastic modulus for soils which experience zero and n freeze-thaw cycles, respectively.

To reflect the coupling effect of load and freeze-thaw, the damage variable D_m was derived as

$$D_m = D + D_n - D \cdot D_n \tag{4}$$

where D_m is the damage variable considering both load and freeze-thaw; D is the damage variable for structural damage induced by load; $D \cdot D_n$ denotes the possible reinforcement when a certain load was applied on the freeze-thaw soils.

Substituting the expression of D_n and D into D_m, we get

$$D_m = 1 - \frac{E_n}{E_0} e^{-\left(\frac{F}{F_0}\right)^{\beta}} \tag{5}$$

According to the Lemaitre principle, the damage model can be written as

$$\boldsymbol{\sigma} = \left(1 - D_m\right) E\boldsymbol{\varepsilon} \tag{6}$$

Substituting Eq. (5) into Eq. (6), we obtain

$$\boldsymbol{\sigma} = e^{-\left(\frac{F}{F_0}\right)^{\beta}} E_n\boldsymbol{\varepsilon} \tag{7}$$

As far as the conventional triaxial stress state is concerned, Eq. (7) can be written as

$$\sigma_1 - 2\mu\sigma_3 = E_n\varepsilon_1 e^{-\left(\frac{F}{F_0}\right)^{\beta}} \tag{8}$$

where σ_1 and σ_3 are the maximal and minimal principle stresses; μ is the Poisson's ratio.

The Drucker-Prager strength criterion is used to represent the damage in soil elements. Let us consider a triaxial test under constant confining pressures, we firstly select the stress state before any deviatoric stress is applied, while the second is chosen to be the stress state when a peak stress is reached. So the following conditions should be satisfied

$$\sigma_1 = 0, \quad \frac{d\sigma_1}{d\varepsilon_1} = E \quad when \quad \varepsilon_1 = 0; \tag{9}$$

$$\sigma_1 = \sigma_P, \quad \frac{d\sigma_1}{d\varepsilon_1} = 0 \quad when \quad \varepsilon_1 = \varepsilon_P \tag{10}$$

where ε_P is the strain at which the peak stress σ_P is reached.

By differentiating Eq. (8), we obtain the following equation

$$\frac{d\sigma_1}{d\varepsilon_1} = E_n e^{-\left(\frac{F}{F_0}\right)^{\beta}} \left\{1 + \varepsilon_1 \left[-\beta\left(\frac{F}{F_0}\right)^{\beta-1}\right] \frac{1}{F_0} \frac{\partial F}{\partial \varepsilon_1}\right\} \tag{11}$$

Substituting Eqs. (9) and (10) into Eqs. (8) and (11), the parameters β and F_0 can be deduced as

$$\beta = -\frac{1}{\ln \dfrac{\sigma_p}{E_n\varepsilon_p}} \tag{12}$$

$$F_0 = \left(\beta F_p^{\beta}\right)^{1/\beta} \tag{13}$$

where F_p is the value of F when the peak stress is reached.

2.2 Thaw consolidation

The heat transfer during thaw consolidation of frozen ground is a strongly nonlinear problem due to ice-water phase change. The heat transfer equation for frozen soils can be written as

$$-h_{i,i} + h_v = \rho C \frac{\partial T}{\partial t} \tag{14}$$

where h_v is the volumetric heat source intensity; h_i is the heat flux vector defined as $h_i = -T_{,i}$; ρ is the density of medium; C and λ are equivalent specific heat and thermal conductivity, respectively.

The thermal indexes C and λ in the phase-change temperature range $[T_b, T_p]$ can be defined as

$$C = C_f + \frac{C_u - C_f}{T_p - T_b}\left(T - T_b\right) + \frac{L}{1+W}\frac{\partial W_i}{\partial T} \tag{15}$$

$$\lambda = \lambda_f + \frac{\lambda_u - \lambda_f}{T_p - T_b}\left(T - T_b\right) \tag{16}$$

where f and u denote frozen and unfrozen states of soils, respectively; W and W_i are the contents for water and ice, respectively.

Assuming that the vapor and ice flow are negligible and the transportation and deposition of soil particles during consolidation are not considered, a modified Richards' equation for steady or unsteady fluid flow in a saturated or partially saturated soil during freezing can be written as (Watanabe and Wake 2008)

$$\frac{\partial W_w}{\partial t} = \frac{\partial}{\partial z}\left(k(h)\frac{\partial h}{\partial z} + k(h) + k(h)\gamma h\frac{\partial T}{\partial z}\right) \tag{17}$$

where W_w is the equivalent liquid water content; z is a spatial coordinate; h is the water pressure head; γ is the surface tension of soil water.

The value of h in unfrozen soils can be determined from water retention curves for fine sand while for frozen domain it is estimated by the generalized Clausius-Clapeyron equation. Here, we assumed the ice pressure is equal to zero gauge pressure (Hansson *et al*. 2004), thus a simplified form was deduced as

$$\frac{dP}{dT} = \frac{L_f}{v_w T} \tag{18}$$

where P is the pressure ($P = \rho_w g h$), with g as the acceleration of gravity; L_f is the latent heat during soil freezing; v_w s the specific volume of water.

The hydraulic conductivity for unsaturated frozen sand can be written as (Watanabe and Wake 2008)

$$k(h) = -\frac{J_w}{\frac{\Delta T}{\Delta z}\gamma h + \frac{\Delta h}{\Delta z} + 1} \tag{19}$$

where J_w denotes the water flux obtained from the derivative of equivalent water content W_w with respect to time t. The equivalent water content W_w can be deduced as

$$W_w = W_u + \frac{\rho_i}{\rho_w} W_i \tag{20}$$

where $W_u = f(T)$ can be empirically determined by (Ma and Wang 2014)

$$W_u = a\left|T\right|^{-b} \tag{21}$$

where a_1 and b_1 are experimental coefficients.

Considering the compressibility of fluid and soil particles, the conservation equation can be written as

$$-q_{i'i} + q_v = \frac{1}{M}\frac{\partial p}{\partial t} + \alpha \frac{\partial \varepsilon_v}{\partial t} \tag{22}$$

where q_v is the volumetric fluid source intensity; $\varepsilon_v = \varepsilon_{ii}$ ($i = 1 - 3$); α is the Biot's coefficient; M is the Biot's modulus. If the compressibility of soil particles is negligible, α is equal to 1.0 and M can be estimated by K_w/n, in which K_w is the fluid bulk modulus and n is the porosity of soils.

Following the work by Wang *et al*. (2013), the 3D theory for thaw consolidation proposed by Yao *et al*. (2012) was improved by introducing the Drucker-Prager yield criterion to describe the mechanical behaviors of post-thawed soils

$$\alpha_1 I_1 + \sqrt{J_2} = k_1 \tag{23}$$

where I_1 and J_2 are the first invariant of principle stress and second invariant of deviatoric stress, respectively; The parameters α_1 and k_1 are defined as

$$\alpha_1 = \frac{2\sin\varphi}{\sqrt{3}\left(3-\sin\varphi\right)}, k_1 = \frac{6c\cos\varphi}{\sqrt{3}\left(3-\sin\varphi\right)} \tag{24}$$

where c and φ are the cohesion and angle of internal friction.

The motion of soil element can be described by the balance of its linear momentum

$$\sigma_{ij'j} + \rho g_i = \rho \frac{dv_i}{dt} \tag{25}$$

In the Eulerian description, the symmetric strain rate tensor and the skew-symmetric spin tensor are given as

$$\dot{\varepsilon}_{ij} = \left(\frac{\partial v_i}{\partial x_j} + \frac{\partial v_j}{\partial x_i}\right)\Big/2 \quad , \dot{w}_{ij} = \left(\frac{\partial v_j}{\partial x_i} - \frac{\partial v_i}{\partial x_j}\right)\Big/2 \tag{26}$$

where v_i (i = 1, 2 and 3) is the instantaneous velocity of the material point. The Jaumann stress rate is used to eliminate the effect of rigid rotation

$$\overset{\vee}{\sigma}_{ij} = \frac{d\sigma_{ij}}{dt} - \sigma_{ik}\,\omega_{ki} - \sigma_{jk}\,\omega_{kj} \tag{27}$$

2.3 Creep of soils

Creep of underlying permafrost layer should be taken into account in estimating settlement of foundations in cold regions, especially when warm frozen soils are involved (Qi *et al*. 2007). Following the work by Wang *et al*. (2014), the creep model combining three typical mechanical elements such as Maxwell body, Kelvin body and Bingham body can be expressed as

$$\varepsilon_{ij} = \frac{\sigma_{ij}}{E_M} + \frac{\sigma_{ij}}{\eta_M}t + \frac{\sigma_{ij}}{E_K}\left[1 - \exp\left(-\frac{E_K}{\eta_K}t\right)\right], \qquad \phi(F) \le 0 \tag{28a}$$

$$\varepsilon_{ij} = \frac{\sigma_{ij}}{E_M} + \frac{\sigma_{ij}}{\eta_M}t + \frac{\sigma_{ij}}{E_K}\left[1 - \exp\left(-\frac{E_K}{\eta_K}t\right)\right] + \frac{1}{\eta_N}\left\langle\phi\left(F\right)\right\rangle\frac{\partial Q}{\partial\{\sigma\}}t, \qquad \phi(F) > 0 \tag{28b}$$

where E_M and E_K are elastic modulus for Maxwell and Kelvin bodies, respectively; η_M, η_K and η_N are the coefficients of viscosity for Maxwell body, Kelvin body and Bingham body; and Q is a viscoplastic potential function. $\phi(F)$ is the scaling function representing the magnitude of creep stage, which can be written as

$$\phi\left(F\right) = \left\langle\frac{F}{F_0}\right\rangle \tag{29}$$

where F_0 is the reference value, equal to 1.0 MPa for frozen soils. In the case of $\phi(F) \le 0$, the model is actually the Burgers model while the viscoplastic strain represented by the Bingham body is taken into account when $\phi(F) > 0$.

Further studies indicate that the parabolic yield criterion is more applicable for the shear yield of frozen soils within a wide range of stress levels (Fish 1991) and the basic formula of F is defined as

$$F = \sqrt{3J_2} - c - \sigma_m\tan\varphi + \frac{\tan\varphi}{2p_m}\sigma_m^2 \tag{30}$$

where p_m is the mean normal stress corresponding to the maximum shear stress q_m; and σ_m and J_2 are first principal stress invariant and second deviatoric stress invariant, respectively. For simplicity, the associated flow rule is employed here and we assumed that the viscoplastic potential $Q(\sigma_{ij})$ has the same form of the yield function $F(\sigma_{ij})$.

3. Numerical method

3.1 Key technical problems

Three main sources of settlement in foundations in cold regions will vary with heat budget in

atmosphere. In the warm season, the drainage paths from post-thawed domain to ground surface are unblocked, and thaw consolidation of frozen soils occurs in the post-thawed area while in warm and cold permafrost layers beneath the post-thawed, creep accounts for a major part of the total deformation. When drainage paths are blocked in cold season, consolidation of post-thawed soils ceased to develop and creep of soils is the primary source. When freeze-thaw cycling is involved, the additional settlement due to the variation of the engineering properties of soils should be taken into account.

One of key technical problems for analyzing these complex processes is to detect the computational domains for thaw consolidation and creep. Following the work by Wang *et al*. (2013), the procedures for live detecting domains for thaw consolidation and creep are as follows. Firstly, a loop code was compiled to determine whether temperatures for elements on drainage boundaries are higher than zero or not. If so, drainage paths are unblocked and constitutive models for thaw consolidation are used in post-thawed domain, with creep model assigned in frozen area. In this case, the hydraulic and mechanical modes are activated in post-thawed domain (i.e., set ther off fluid on mech on) while only the mechanical is activated in frozen area (i.e., set ther off fluid off mech on). Otherwise, only the creep model is assigned in the whole domain and the mechanical mode is activated while the thermal and hydraulic modes were turned off (i.e., set ther off fluid off mech on).

The second is to synchronize water and heat coupling calculations. For cases when drainage paths are unblocked, the timesteps for thermal and hydraulic calculations during thaw consolidation are selected as *th*dt = *N*·*fluid*dt when performing a coupled analysis. Moreover, the critical timesteps should be satisfied to ensure the stabilization (Itasca 1999)

$$\begin{cases} fluid\mathrm{dt}_{cr} \le \dfrac{L_c^2}{c_{fluid}} \\ th\mathrm{dt}_{cr} \le \dfrac{L_c^2}{c_{th}} \end{cases} \tag{31}$$

where $fluid\mathrm{dt}_{cr}$ and $th\mathrm{dt}_{cr}$ are the critical timesteps for the hydraulic and thermal calculations, respectively; L_c is the characteristic length; c_{fluid} and c_{th} are the hydraulic and thermal diffusivity, respectively.

Otherwise, we should synchronize thermal and mechanical calculations in frozen domain by trial and the following equation should be satisfied

$$\frac{\Delta t_{ther}}{\Delta t_{mech}} = \sqrt{\frac{\rho}{K + (4/3)G}}\,\frac{L_c}{c_{th}} \tag{32}$$

where Δt_{ther} and Δt_{mech} are timesteps for thermal and mechanical calculation; ρ is the density of material; K and G are the bulk and shear modulus, respectively.

The last is live detecting computational domain which experiences freeze-thaw cycling. The engineering properties for elements marked as freeze-thaw will be updated as well. Here, we firstly record the data of temperature field for each element in the whole domain by iterating over all elements. Then the judgment statement for detecting whether freeze-thaw occurs or not can be expressed as

$$f(T_i) = T_i^{\tau-1} \times T_i^{\tau} \tag{33}$$

where $T_i^{\tau-1}$ and T_i^{τ} are temperatures for element i at time $\tau - 1$ and τ, respectively.

If $f(T_i) > 0$, the number of freeze-thaw cycles N_i should not be updated for element i; otherwise, it will be updated as $N_{i+1} = N_i + 1$. Before computation, the number of freeze-thaw cycles for each element is assigned zero. For elements which undergo a certain number of freeze-thaw cycles, the statistical damage model is assigned and corresponding engineering indexes such as elastic modulus and cohesion will be live updated. From this perspective, the additional settlement induced by freeze-thaw in seasonal active layer can be simulated.

3.2 Computational procedure

The code for analyzing settlement of foundations in cold regions was compiled in the built-in FISH language on the FLAC platform. The specific procedures illustrated in Fig. 1 are as follows

(1) Thermal indexes considering latent heat released or absorbed during ice-water phase change are assigned for each element according to the initial thermal state such as the specific heat $C(T)$ and the coefficient of heat conductivity $\lambda(T)$. Turning off hydraulic and

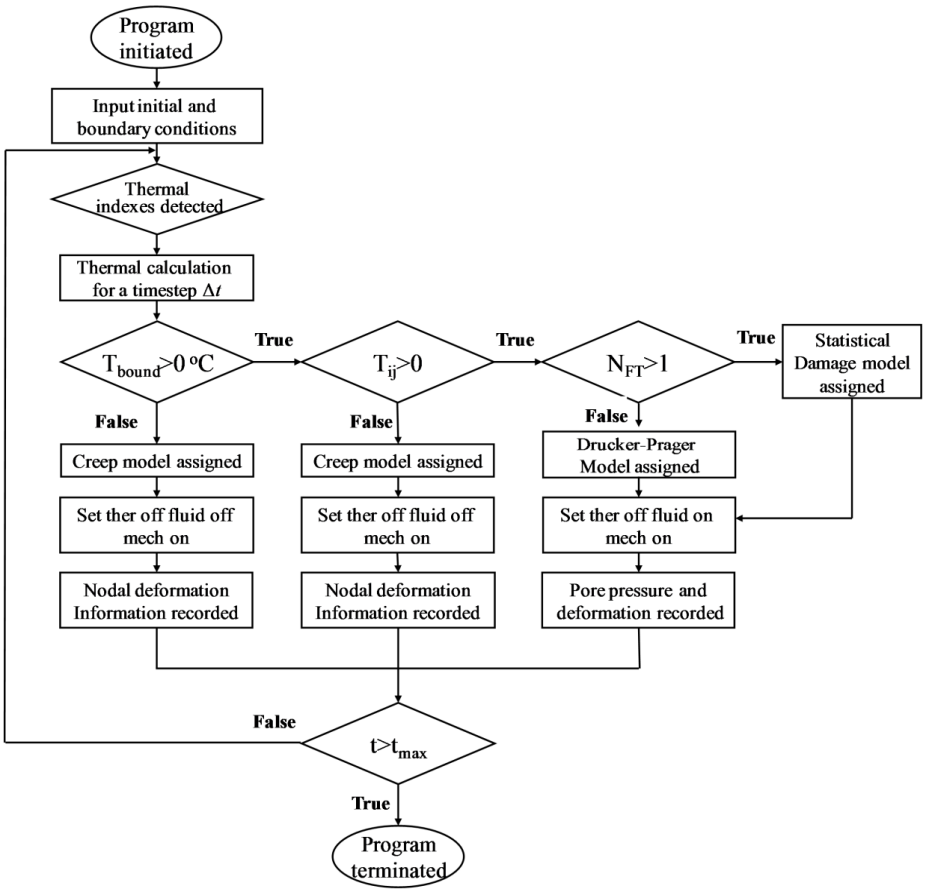

Fig. 1 Computational procedures for settlement analysis

mechanical modes, one step of thermal calculation is carried out, i.e., set ther on mech off fluid off, with the time of t_{ther};

(2) Detect whether drainage paths are blocked or not. Note that the drainage paths for highways include slopes of embankments and natural ground surface while the pavements should also be considered for railways;

(3) If the drainage paths are unblocked, the number of freeze-thaw cycles $N_{FT}(i, j)$ should be detected for elements (i, j) with $T_{element} \geq 0°C$. For the newly thawed soils, the Drucker-Prager model is assigned while the statistical damage model considering both freeze-thaw cycling and load assigned in elements which experience cyclic freeze and thaw. Then for post-thawed domain, the hydraulic and mechanical modes are turned on (i.e., set ther off mech on fluid on) with the time equal to thermal calculation duration, i.e., $t_{con} = t_{ther} = N_{con}*\Delta t_{con}$. For elements with temperatures lower than 0°C, the creep model is assigned and only the mechanical mode is set on (i.e., set ther off mech on fluid off), with the time of $t_{creep} = t_{ther} = N_{creep}*\Delta t_{creep}$, where N_{creep} is the number of steps for creep calculation and Δt_{creep} is the corresponding timestep;

(4) If drainage paths are blocked, i.e., in cold season, only the creep analysis is carried out in frozen and unfrozen domains. As for elements with $T_{element} > 0°C$, creep model for post-thawed soils is assigned while for elements in frozen state, i.e., $T_{element} < 0°C$, the model for frozen soils was given. Thus, the thermal and hydraulic modes are turned off and only the mechanical is activated (i.e., set ther off mech on fluid off), with the time of $t_{creep} = t_{ther} = N_{creep}*\Delta t_{creep}$;

(5) When hydraulic and mechanical modes are terminated, the computational results for nodes and elements within this timestep are recorded. The whole domain is reassigned by new thermal indexes determined by thermal regime in this timestep.

(6) Determine whether the target time is reached or not. If true, the program is terminated, with the recorded data processed; otherwise, the cycle from step (1) to (5) will be implemented until the target time.

4. Experimental verification

4.1 Test program

The test data in literature (Ma and Wang 2014) was used to verify the proposed numerical method. The sandy clay along Qinghai-Tibet railway was taken as the study object. The dry density for sandy clay is 1.40 g·cm^{-3} and the initial water content is 20.9%. The grain size distribution curve is illustrated in Fig. 2.

The cylindrical samples were produced by slowly compacting slurry in a high strength organic glass tube. The diameter for soil specimen is 100 mm and the height is 112.8 mm. Due to the negative effect of soluble salt on freeze-thaw process of soils, the distilled water was used to prepare soil samples. To observe the development of 0°C isothermal line, the thermistor thermometer was placed in specimen in the vertical direction with the interval of 2.0 cm. During testing the thermal insulation sponge was wrapped around organic glass tube to ensure the unidirectional freeze and thaw in soil specimen. Moreover, the displacement sensors were set up in the upper part. The data can be live recorded by data logger, with an accuracy of ± 0.01 mm.

The freeze-thaw testing apparatus include the following parts such as thermostat, sample box,

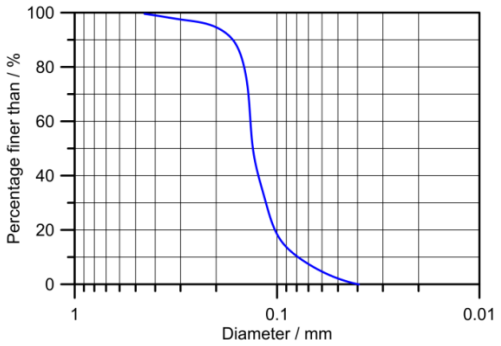

Fig. 2 Grain size distribution curve for sandy clay

loading device, supply systems for circulated fluid and water, measuring systems for temperature and displacement, and heat insulation. The thermostat can live adjust the temperatures inside. The sample box consists of three main parts, i.e., upper and bottom ends and organic glass tube, of which both upper and bottom ends sealed by asbestos paper have similar structure with holes for circulating fluid tubes and water supply system. The external water can be live supplied to soil sample through both ends. The stress can be applied on soil specimen by the loading device through the upper end. The water supply system includes a fine glass tube with small index value to adjust the inflow of external water.

The procedures for testing are as follows: (i) prepare soil samples according to target water content and dry density in organic glass tube and place the thermistor thermometer in corresponding locations in specimen with heat insulated sponge wrapped around the tube; (ii) Set up displacement sensor on upper end of sample box and the fine glass tube for water supply system was connected as well as the warm and cold circulating fluid; (iii) Adjust the temperature for upper end to be −5.0 − +5.0°C every three hours while for bottom end and thermostat inside to be +1.0°C; (iv) After testing, the redistribution of water was obtained by measuring water content for each layer. The freeze-thaw test was carried out under no load and the inflow of external water is available.

4.2 Numerical model

The geometric model for computation is identical to that of freeze-thaw test, with height of 100 mm and diameter of 112.8 mm. The displacement in x direction is fixed for both sides while for bottom side the displacement in y direction is constrained and for upper displacement free. Moreover, both sides of the model are assumed adiabatic with nodal temperatures fixed. For the bottom end a constant temperature is applied while for the upper a simplified thermal boundary presented in Fig. 3 is used, which can be written as

$$T_{upper} = l\sin(wt + \theta_0) \tag{34}$$

where l is the amplitude of thermal boundary; w is the frequency; θ_0 is the initial phase. From the measured data the parameters can be fitted, i.e., $l = 5.0$°C; $w = 1.047$; $\theta_0 = \pi/2$.

At a constant warm-end temperature, the inflow R_w from the bottom of soil sample can be empirically estimated by the following equation (Ma and Wang 2014)

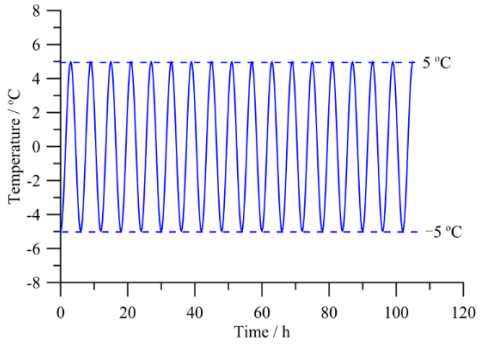

Fig. 3 The temperatures for upper end of specimen

Table 1 The physical parameters for sand clay

Soil type	ρ_d/ g/cm^3	W /%	C/J/kg·°C		λ/W/m·°C		K/10^{-7}m/s
			Frozen	Thawed	Frozen	Thawed	
Sandy clay	1.4	20.9	1670	1380	0.94	1.00	6.12

Table 2 The specific heat for sandy clay

T/°C	20.0-0.0	0.0-—0.2	—0.2-—0.5	—0.5-—1.0	—1.0-—2.0	—2.0-—3.0	—3.0-—5.0	—5.0-—10.0	—10.0-—20.0
C/J/kg·°C	1672	90452	33412	11057	6223	6148	2518	1618	1380

$$R_w = 1.356 \times 10^{-7} T^{1/2} \tag{35}$$

At a constant warm-end temperature, the inflow R_w from the bottom of soil sample can be empirically estimated by the following equation (Ma and Wang 2014).

The hydraulic conductivity for soils at various temperatures can be expressed as (Chen *et al*. 2006)

$$K(T) = K(T_{ref}) \frac{\mu(T_{ref})}{\mu(T)} \tag{36}$$

where $\mu(T)$ is the coefficient of viscosity for water at a temperature of T; T_{ref} is the reference temperature.

The coefficients of viscosity for water at various temperatures are listed in Table 3.

From previous work we found that the hydraulic conductivity for fine-grained soils after freeze and thaw generally increases (Qi *et al*. 2006). In this study we assumed that the hydraulic conductivity for sandy clay will increase by two orders of magnitude after fifteen freeze and thaw cycles and afterwards it tends to stabilize. Table 4 presents the hydraulic conductivity for sandy clay at a certain number of freeze-thaw cycles.

The mechanical properties for frozen soils will vary with temperatures such as elastic modulus E, Poisson's ratio v, cohesion c and angle of internal friction φ (Ma and Wang 2014). From experimental results, Li *et al*. (2009a) proposed the following empirical equations to describe

Table 3 Coefficients of viscosity at various temperatures

T/°C	20	10	0	−2	−5	−10
$\mu/10^{-3}$ Pa·s	1.00	1.31	1.79	1.91	2.14	2.60

Table 4 Hydraulic conductivity for sandy clay

N_{FT}	0	1	5	10	15
$K/10^{-6}$cm/s	0.61	1.47	11.1	31.9	61.2

the mechanical properties for frozen soils at various temperatures

$$\begin{cases} E = a_1 + b_1 \left|T\right|^m \\ v = a_2 + b_2 \left|T\right| \\ c = a_3 + b_3 \left|T\right| \\ \varphi = a_4 + b_4 \left|T\right| \end{cases} \tag{37}$$

where a_i and b_i are empirical coefficients (i = 1-4); m is a parameter related to soil temperature, equal to 0.6 for frozen soils. The mechanical properties for sandy clay at various temperatures are shown in Table 5.

From Eq. (33) we observed that the mechanical properties of frozen soils include two main parts, i.e., the component for post-thawed and that strongly dependent on soil temperature. Here, we assumed only the former component is influenced by freeze-thaw cycling. The mechanical properties for sandy clay after N freeze-thaw cycles are listed in Table 6.

The parameters for the creep model can be fitted from experimental results (Ma and Wang 2014, Zheng *et al*. 2010), as listed in Table 7.

Table 5 The mechanical properties for sandy clay at various temperatures

T/°C	−15	−10	−5	−3	−1	0	15
E/MPa	3.36	2.76	2.01	1.63	1.12	0.57	0.57
v	0.28	0.32	0.36	0.37	0.39	0.40	0.40
c/MPa	0.96	0.70	0.45	0.34	0.24	0.15	0.15
φ/°	36	28	20	17	14	12	12

Table 6 The mechanical properties for sandy clay after N freeze-thaw cycles

N_{FT}	0	3	5	7	10	15
E/MPa	0.57	0.25	0.20	0.18	0.18	0.28
μ	0.40	0.40	0.40	0.40	0.40	0.40
c/MPa	0.15	0.17	0.18	0.19	0.20	0.20
φ/°	12	12	12	12	12	12

Table 7 Creep parameters for sandy clay

T/°C	10	−0.2	−0.5	−1	−2	−5
G_k/MPa	0.24	0.44	0.69	1.16	1.51	1.65
$\eta_K/10^5$MPa·d	0.32	0.59	0.92	1.55	2.02	2.20
G_M/MPa	0.49	0.89	1.39	2.34	3.05	3.33
$\eta_M/10^3$MPa·d	0.44	0.80	1.25	2.12	2.75	3.01

4.4 Comparison of numerical and test results

Here, the temperature profile of soil specimen was taken to investigate how thermal regime develops. For sake of safety we select the temperature profile at the time when a maximum value was applied on the upper end, as presented in Fig. 4. We can see from the figure that frozen soil specimen thaws from both ends and the domain in frozen state tends to decrease after cyclic freeze-thaw, indicating a gradual increase in temperature in soil specimen.

For further detecting the variation of thermal regime, four nodes along the height of the computational model were selected. The distances for four nodes A, B, C and D from the bottom end are 8.0, 6.0, 4.0 and 2.0 cm. We can see from Fig. 5 that at a given sinusoidal temperature boundary, the nodes in soil specimen all show similar changes in temperature, manifesting as

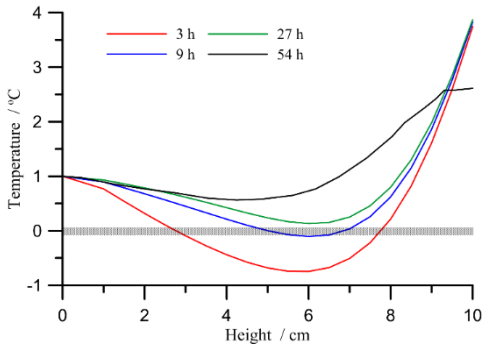

Fig. 4 Temperature profile of soil specimen

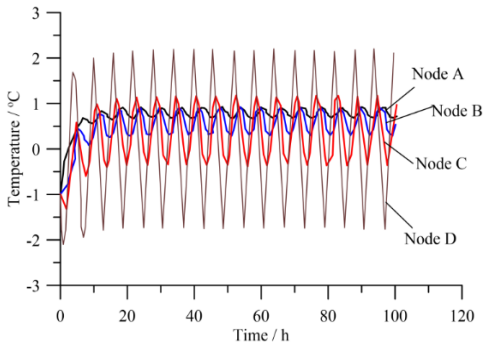

Fig. 5 Variation of temperatures for four nodes

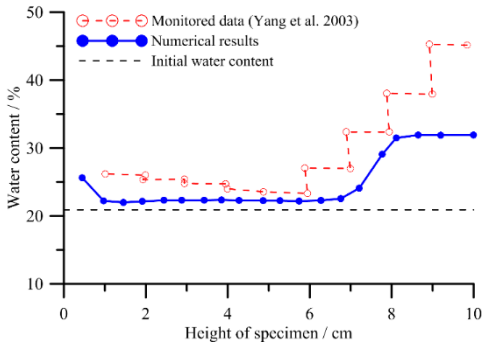

Fig. 6 Water content profile for soil specimen

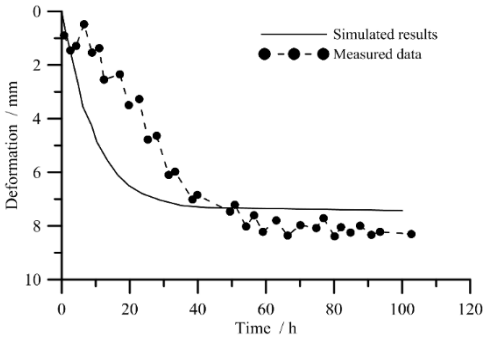

Fig. 7 Comparison of simulated and measured deformation

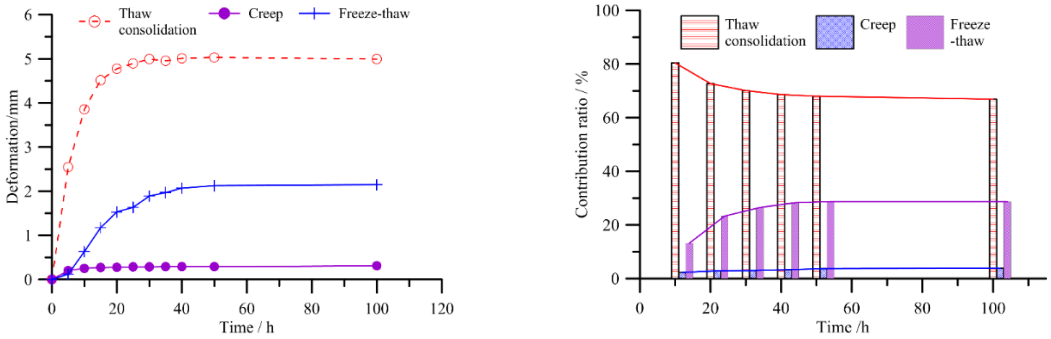

(a) Magnitude of deformation (b) Proportion of each source

Fig. 8 The proportion of each source in total deformation

relatively stable sinusoidal variations accompanied by an instable stage in the initial three to five freeze and thaw cycles. Besides, the temperatures for nodes close to the upper end are rather larger.

Comparison of simulated and measured profile for water content is shown in Fig. 6. The water content in the upper part of soil specimen obviously increases after freeze and thaw testing compared with that in the bottom, indicating a significant migration of water in sandy clay, which is closely related to the water supplemented from the bottom due to temperature gradient during

freezing.

The comparison between simulated and measured deformation is presented in Fig. 7. Due to the fact that the frost heave during soil freezing is not taken into account, the compression of soil sample dominates the whole process. From the figure we noticed that the simulated results agree in general with test data.

The procedure for determining the proportions of each source in total deformation is suggested as follows:

(1) Calculate the total deformation ε_T considering coupling effects of thaw consolidation, creep and freeze-thaw cycling;
(2) Calculate the deformation induced by both thaw consolidation and creep $\varepsilon_{F\text{-}T}$ without considering freeze-thaw. So the deformation caused by freeze-thaw cycling is equal to the difference between ε_T and $\varepsilon_{F\text{-}T}$;
(3) Fix the nodal displacement in elements in frozen state, and only thaw consolidation of post-thawed domain is carried out. So the proportion of thaw consolidation in the total deformation can be obtained, marked as $\varepsilon_{T\text{-}C}$;
(4) Creep deformation of sandy clay ε_C is equal to ε_T—$\varepsilon_{F\text{-}T}$—$\varepsilon_{T\text{-}C}$.

The proportion of each source in the total deformation is illustrated in Fig. 8. We can see that for sandy clay thaw consolidation accounts for a major part of the total deformation, especially in the initial five freeze-thaw cycles; however, it tends to stabilize afterwards. For cases when no external load is applied, creep of soil is relatively small during testing. Besides, freeze-thaw induced deformation obviously affects the initial stage during testing but afterwards it tends to diminish.

5. Simulation of a model test

5.1 Design of model test

The model test carried out by Yu *et al*. (2014) was used to verify the rationality of the proposed numerical method. The frequently encountered silty clay in the Qinghai-Tibet plateau was used in model test. The liquid and plastic limits for the silty clay are 24.5% and 14.5%, respectively. The model test includes three main parts, i.e., a concrete tank, a temperature controlling system and a loading system. A half embankment model with height of 1.0 m and length of 2.5 m was constructed by silty clay layer by layer into a concrete tank with length of 3.0 m, width of 2.5m, and depth of 1.5 m. The target water content is 16.5 % and the density is 1.7 g/cm^3 corresponding to the soil density in situ. It consists of a 0.75 m-high embankment body and a 0.25 m-high active layer.

Before testing, the 100 cm thick styrofoam insulating layers was placed in concrete walls with a removable top cover plate and the soil surface was covered by a plastic film to reduce the evaporation of soil water. Moreover, the temperatures for the cooling plates placed on top, slope and bottom of the model was controlled by a refrigerating circulator and an external load of 10 kPa was applied by almost 1.7 ton iron blocks. The ground temperatures of the embankment model were monitored by temperature sensors. Four displacement sensors were used to monitor the settlement at top cooling plate. The range for temperature sensor is —50-260°C, with an accuracy of ± 0.05°C while for displacement sensor the range is 0-50 mm, with an accuracy of ± 0.04 mm.

As for the specific layout for temperature and displacement sensors in the model test, please refer to the literature (Yu *et al*. 2014).

The model test includes three main steps: (i) the temperatures for cooling plates for top, slope and bottom were set to be —20, —20 and —5°C in order to simulate the freezing process due to cold weather and the heat transfer from cold permafrost layer, with a duration of 19 d, corresponding to the cold seasons; (ii) Stop the temperatures for top and slope plates and the bottom was set to be —1°C; in the meanwhile, the heat bulbs above started to work, with the time of 15 d, so as to simulate the process of freezing upwards due to heat transfer from warm permafrost layer, and thawing downwards caused by warm weather, corresponding to the warm season; (iii) Adjust the temperatures for top, slope and bottom to be —2, —1 and —2°C and then a load of 10 kPa was applied on the top cooling plate. This process simulated the creep of permafrost. During testing no external water is supplied to the embankment model.

5.2 Geometric model

The geometric model for computation is identical to that of a half embankment model, as illustrated in Fig. 9(a). The temperatures for top, slope and bottom cooling plates are applied in accordance with those in the model test during the three stages. Considering that no external water is supplied in embankment model, the permeability of the bottom is assumed to be zero while the top and slope are drainage boundaries. The *x*-displacement is fixed for both sides of the model while the *y*-displacement of the bottom side is constrained. The upper boundary is assumed to be displacement free. Besides, both sides of the model are assumed adiabatic with nodal temperatures fixed.

5.3 Parameter determination

Considering the variation of unfrozen water of frozen soil during phase change, the physical parameters for silty clay are presented in Tables 8 and 9. Here, the frozen soil is assumed impermeable and the water migration occurs only in the post-thawed domain. According to the experimental results in literature (Ma and Wang 2014), the mechanical parameters for silty clay are listed in Table 10. Creep parameters for silty clay were obtained from test results (Ma and Wang 2014, Zheng *et al*. 2010), as shown in Table 11.

Table 8 Physical parameters for silty clay

Stratum	ρ_d/ g/cm^3	W /%	K*/ m/h	a/ %/°C	b	λ/ W/(m·°C)	
						Frozen	Thawed
Silty clay	1.7	16.5	1.7×10^{-10}	10.217	0.242	1.45	0.86

Table 9 The equivalent specific heat for silty clay

T /°C	20.0～0.0	0.0～−0.2	−0.2～−0.5	−0.5～−1.0	−1.0～−2.0	−2.0～−3.0	−3.0～−5.0	−5.0～−10.0	−10.0～−20.0
Silty clay	1794	130278	35903	11864	6678	6640	2702	1737	1283

Table 10 Mechanical parameters for silty clay

Stratum	Elastic parameters	T/°C							
		-20	-10	-5	-2	-1	-0.05	0	20
Silty clay	E/MPa	262.5	127.5	66	27.7	4.9	1.1	0.75	0.75
	v	0.15	0.15	0.18	0.2	0.22	0.24	0.4	0.4

Table 11 Creep parameters for silty clay

Stratum	T/°C	E_M/MPa	E_K/MPa	η_M/MPa·h	η_K/MPa·h	η_N/MPa·h
Silty clay	−20	234.22	61.59	5866.69	483.25	329.68
	−5	144.48	25.47	2416.58	32.97	17.43
	−1	120.54	15.84	1496.25	16.11	7.96
	0	114.56	13.43	1266.43	13.47	6.54
	20	95.69	11.56	1159.02	12.59	5.70

Table 12 The parameters for silty clay after N freeze-thaw cycles

N_{FT}	0	1	5	10	15
K/10^{-6}cm/s	0.02	0.61	1.47	11.1	41.9
E/MPa	0.75	0.32	0.27	0.23	0.23
c/MPa	0.35	0.27	0.23	0.21	0.21

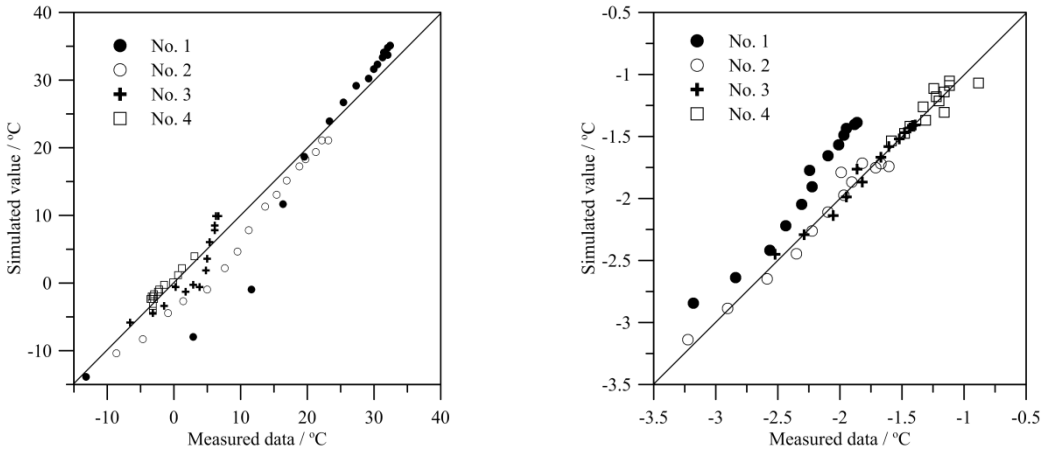

(a) Thawing process (b) Creep

Fig. 9 Comparison of measured and simulated temperatures during thawing

As for silty clay the Poisson's ratio and the angle of internal friction are assumed to be constant after freeze-thaw cycling. In this study the Poisson's ratio is taken to be 0.35 and the angle of internal friction is 15°. Moreover, based on previous experimental results the parameters for silty clay after N freeze-thaw cycles were listed in Table 12.

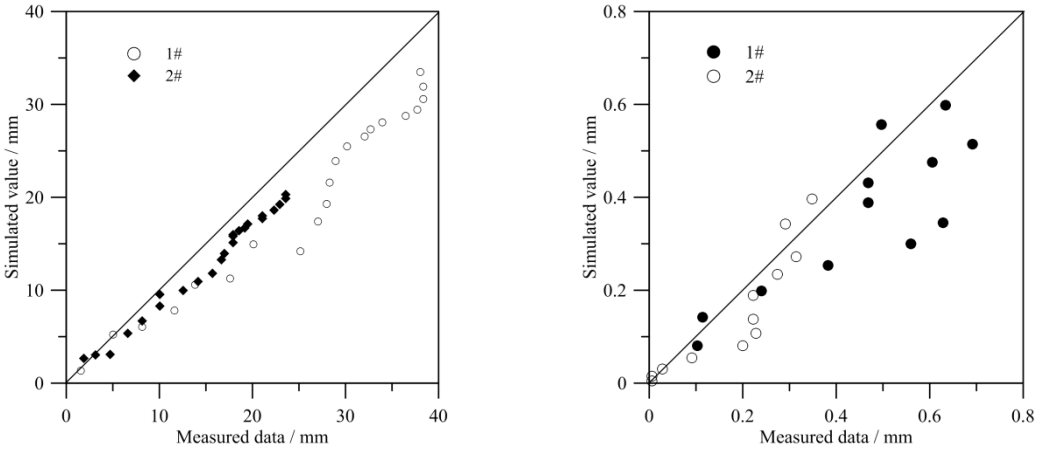

(a) Thawing process (b) Creep

Fig. 10 Comparison of measured and simulated deformation during thawing

5.4 Comparison of calculated and measured data

In this study, the frost heave of the embankment model during freezing process is not considered and only the settlement of the embankment model is introduced here. Fig. 9 presents the comparison of simulated and measured nodal temperature variations during thawing and creep processes. We can see from the figure that most of the data points lies around the $y = x$ line, indicating that the simulated temperatures agree well with measured data.

Moreover, the comparison between simulated and measured deformation of the embankment model during thawing and creep processes are illustrated in Fig. 10. It shows that for the two monitoring points 1# and 2#, the deformation simulated coincides in general with that measured during testing.

6. Conclusions

In this paper, a novel numerical method was put forward for settlement analysis of embankments in cold regions by taking into account freeze-thaw cycling, thaw consolidation and creep. The theoretical models for the three sources of settlement were established including a statistical damage model for soils which experiences cyclic freeze and thaw, a large strain thaw consolidation theory incorporating a modified Richards' equation and a Drucker-Prager yield criterion, and a simple rheological element based creep model for frozen soils.

The key technical problems including synchronization of water and heat coupling calculations, and live detecting computational domains for freeze-thaw cycling, thaw consolidation and creep were conveniently solved by compiling a section of codes by using the built-in language FISH on the FLAC platform.

This method is firstly verified by freeze-thaw tests on sandy clay taken from Qinghai-Tibet plateau. Results show that the simulated results agree in general with test data. The contributions of the three sources were separated from the total settlement and we observed that thaw consolidation accounts for a major part, followed by freeze-thaw cycling while creep only

occupies a small portion. Then an embankment model test performed on a frequently encountered silty clay along the Qinghai-Tibet highway was modeled and a good correlation between calculated and measured data was observed.

Acknowledgments

The research described in this paper was financially supported by the National Natural Science Foundation of China (51408486 and 41172253), the European project CREEP (PIAPP-GA-2011-286397). These supports are greatly appreciated.

References

Che, A.L., Wu, Z.J. and Wang, P. (2014), "Stability of pile foundations base on warming effects on the permafrost under earthquake motions", *Soils Found*., **54**(4), 639-647.

Chen, X.B., Liu, J.K., Liu, H.X. and Wang, Y.Q. (2006), *Frost Action of Soil and Foundation Engineering*, Science Press, Beijing, China. [In Chinese]

Cheng, G.D., Wu, Q.B. and Ma, W. (2008), "Innovative designs of the permafrost for the Qinghai-Tibet Railway", *Proceedings of the 9th International Conference on Permafrost*, Fairbanks, AL, USA, June-July, pp. 239-245.

Fish, A.M. (1991), "Strength of frozen soil under a combined stress state", *Proceedings of the 6th International Symposium Ground Freezing*, Beijing, China, September, pp. 135-145.

Hansson, K., Šimůnek, J. and Mizoguchi, M. (2004), "Water flow and heat transport in frozen soil: numerical solution and freeze-thaw application", *Vadose Zone J*., **3**(2), 693-704.

Itasca (1999), Flac manual: Theoretical background, Itasca Consulting Group, Minneapolis, MN, USA.

Kamei, T., Ahmed, A. and Shibi, T. (2012), "Effect of freeze-thaw cycles on durability and strength of very soft clay soil stabilized with recycled Bassanite", *Cold Reg. Sci. Technol*., **82**, 124-129.

Kanevskiy, M., Shur, Y., Krzewinski, T. and Dillon, M. (2013), "Structure and properties of ice-rich permafrost near Anchorage Alaska", *Cold Reg. Sci. Technol*., **93**, 1-11.

Lai, Y.M., Li, S.Y., Qi, J.L. and Chang, X.X. (2008), "Strength distributions of warm frozen clay and its stochastic damage constitutive model", *Cold Reg. Sci. Technol*., **53**(2), 200-215.

Lai, Y.M., Yang, Y.G., Chang, X.X. and Li, S.Y. (2010a), "Strength criterion and elastoplastic constitutive model of frozen silt in generalized plastic mechanics", *Int. J. Plasticity*, **26**(10), 1461-1484.

Lai, Y.M., Gao, Z.H., Zhang, S.J. and Chang, X.X. (2010b), "Stress-strain relationships and nonlinear Mohr strength criteria of frozen sandy clay", *Soils Found*., **50**(1), 45-53.

Li, S.Y., Lai, Y.M., Zhang, M.Y. and Dong, Y.H. (2009a), "Study on long-term stability of Qinghai-Tibet Railway embankment", *Cold Reg. Sci. Technol*., **57**(2-3), 139-147.

Li, S.Y., Lai, Y.M., Zhang, M.Y. and Jin, L. (2009b), "Seismic analysis of embankment of Qinghai-Tibet railway", *Cold Reg. Sci. Technol*., **55**(1), 151-159.

Li, S.Y., Lai, Y.M., Zhang, S.J. and Liu, D. (2009c), "An improved statistical damage constitutive model for warm frozen clay based on Mohr-Coulomb criterion", *Cold Reg. Sci. Technol*., **57**(2-3), 154-159.

Li, X., Cao, W.G. and Su, Y.H. (2012), "A statistical damage constitutive model for softening behavior of rocks", *Eng. Geol*., **143-144**, 1-17.

Ma, W. and Wang, D. (2014), *Frozen Soil Mechanics*, Science Press, Beijing. [In Chinese]

Ma, W., Qi, J.L. and Wu, Q.B. (2008a), "Analysis of the Deformation of Embankments on the Qinghai-Tibet Railway", *J. Geotech. Geoenviron. Eng*., **134**(11), 1645-1654.

Ma, W., Zhang, L.X. and Wu, Q.B. (2008b), "Control of asymmetrical subgrade temperature with crushed-rock embankments along the permafrost region of the Qinghai-Tibet railway", *Proceedings of the 9th International Conference on Permafrost*, Fairbanks, AL, USA, June-July, pp. 1099-1104.

Ma, W., Feng, G.L., Wu, Q.B. and Wu, J.J. (2008c), "Analyses of temperature fields under the embankment

with crushed-rock structures along the Qinghai-Tibet railway", *Cold Reg. Sci. Technol.*, **53**(3), 259-270.
Ma, W., Cheng, G.D. and Wu, Q.B. (2009), "Construction on permafrost foundations: Lessons learned from the Qinghai-Tibet railroad", *Cold Reg. Sci. Technol.*, **59**(1), 3-11.
Matsumura, S., Miura, S., Yokohama, S. and Kawamura, S. (2015), "Cyclic deformation-strength evaluation of compacted volcanic soil subjected to freeze-thaw sequence", *Soils Found.*, **55**(1), 86-98.
Morgenstern, N.R. and Nixon, J.F. (1971), "One-dimensional consolidation of thawing soils", *Can. Geotech. J.*, **8**(4), 558-565.
Qi, J.L., Pieter, A.V. and Cheng, G.D. (2006), "A review of the influence of freeze-thaw cycles on soil geotechnical properties", *Permafrost Periglac.*, **17**(3), 245-252.
Qi, J.L., Sheng, Y., Zhang, J.M. and Wen, Z. (2007), "Settlement of embankment in permafrost regions in the Qinghai-Tibet Plateau", *Norw. J. Geogr.*, **61**(2), 49-55.
Qi, J.L., Yao, X.L., Yu, F. and Liu, Y.Z. (2012), "Study on thaw consolidation of permafrost under roadway embankment", *Cold Reg. Sci. Technol.*, **81**, 48-54.
Qi, J.L., Yao, X.L. and Yu, F. (2013), "Consolidation of thawing permafrost considering phase change", *KSCE J. Civil Eng.*, **17**(6), 1293-1301.
Tsytovich, N.A. (1975), *Mechanics of Frozen Soil*, McGraw-Hill, New York, NY, USA.
Wang, S.H., Qi, J.L., Yu, F. and Yao, X.L. (2013), "A novel method for estimating settlement of embankment in cold regions", *Cold Reg. Sci. Technol.*, **88**, 50-58.
Wang, S.H., Qi, J.L., Yin, Z.Y., Zhang, J.M. and Ma, W. (2014), "A simple rheological element based creep model for frozen soils", *Cold Reg. Sci. Technol.*, **106-107**, 47-54.
Wang, T.L., Liu, Y.J., Yan, H. and Xu, L. (2015), "An experimental study on the mechanical properties of silty soils under repeated freeze-thaw cycles", *Cold Reg. Sci. Technol.*, **112**, 51-65.
Watanabe, K. and Wake, T. (2008), "Hydraulic conductivity of frozen unsaturated soil", *Proceedings of the 9th International Conference of on Permafrost*, Fairbanks, AL, USA, June-July, pp. 147-152.
Wu, Q.B. and Zhang, T.J. (2008), "Recent permafrost warming on the Qinghai-Tibetan plateau", *J. Geophys. Res.*: *Atmos*, **113**(D13). DOI: 10.1029/2007JD009539
Wu, Qingbai, Dong, X.F. and Liu, Y.Z. (2007), "Responses of permafrost on the Qinghai-Tibet plateau to climate change and engineering construction", *Arct. Antarct. Alp. Res.*, **39**(4), 682-687.
Yang, C.S., He, P., Cheng, G.D., Zhu, Y.L. and Zhao, S.P. (2003), "Testing study on influence of freezing and thawing on dry density and water content of soil", *Chinese J. Rock Mech. Eng.*, **22**(Supp. 2), 2695-2699. [In Chinese]
Yang, M.X., Nelson, F.E., Shiklomanov, N.I., Guo, D.L. and Wan, G.N. (2010a), "Permafrost degradation and its environmental effects on the Tibetan Plateau: A review of recent research", *Earth-Sci. Rev.*, **103**(1-2), 31-44.
Yang, Y.G., Lai, Y.M., Dong, Y.H. and Li, S.Y. (2010b), "The strength criterion and elastoplastic constitutive model of frozen soil under high confining pressures", *Cold Reg. Sci. Technol.*, **60**(2), 154-160.
Yao, X.L., Qi, J.L. and Wu, W. (2012), "Three dimensional analysis of large strain thaw consolidation in permafrost", *Acta Geotech.*, **7**(3), 193-202.
Yu, F., Qi, J.L., Yao, X.L. and Liu, Y.Z. (2012), "Degradation process of permafrost underneath embankments along Qinghai-Tibet Highway: An engineering view", *Cold Reg. Sci. Technol.*, **85**, 150-156. DOI: 10.1016/j.coldregions.2012.09.001
Yu, F., Qi, J.L., Yao, X.L. and Liu, Y.Z. (2013), "In-situ monitoring of settlement at different layers under embankments in permafrost regions on the Qinghai-Tibet Plateau", *Eng. Geol.*, **160**, 44-53.
Yu, F., Qi, J.L. and Yao, X.L. (2014), "Analysis on the settlement of roadway embankments in permafrost regions", *J. Earth Sci.*, **25**(4), 764-770.
Zheng, B., Zhang, J.M. and Qin, Y.H. (2010), "Investigation for the deformation of embankment underlain by warm and ice-rich permafrost", *Cold Reg. Sci. Technol.*, **60**(2), 161-168.
Zhou, J. and Tang, Y.Q. (2015), "Centrifuge experimental study of thaw settlement characteristics of mucky clay after artificial ground freezing", *Eng. Geol.*, **190**, 98-108.

CC